Available online at www.sciencedirect.com
ScienceDirect
Journal of Nuclear Materials 356 (2006) 162–167
journal of nuclear materials
www.elsevier.com/locate/jnucmat

Post-irradiation analysis of SINQ target rods by thermal neutron radiography

Peter Vontobel [a,*], Masayoshi Tamaki [b], Noriaki Mori [b], Takaki Ashida [b], Luca Zanini [a], Eberhard H. Lehmann [a], Matthias Jaggi [a]

[a] *Spallation Neutron Source Division, Paul Scherrer Institut, CH-5232 Villigen-PSI, Switzerland*
[b] *Nagoya University, Department for Nuclear Engineering, Chikusa Ku, Nagoya, Aichi 4648603, Japan*

Abstract

Cylindrical lead rods from the SINQ spallation neutron source target have been investigated by thermal neutron-radiography/-tomography using a setup for highly activated samples and dysprosium loaded imaging plates. 2D radiography and 3D tomography results have been obtained from lead target rods from SINQ Target-5 irradiated for 2 years, corresponding a total proton charge accumulation of 10.85 Ah. This was the only non-destructive evaluation method capable to visualize macroscopic material changes induced by proton and/or neutron irradiation. The size and location of defects were identified and areas of interest could be selected for further destructive testing. The high sensitivity of neutrons for hydrogen makes this technique particularly useful when looking for metal hydrides. The formation of lens-shaped zirconium hydride blisters has been identified at the steel/Zircaloy interface of a lead rod with a combined steel/zircaloy cladding. Qualitative and quantitative information has been derived from this neutron radiography inspection.

1. Introduction

The spallation neutron source SINQ [1] of the Paul Scherrer Institute, Switzerland, is a continuous source driven by a 575 MeV proton beam at high proton current, i.e. actually 1.25 mA. The solid state spallation target consists of an array of lead rods with stainless steel cladding (Fig. 1), cooled by heavy water. In order to enhance the neutron yield, upgrade measures are planned on the accelerator side, intending to increase the proton current on the SINQ target to 2 mA. The lead rod target is being optimized by changing the cladding material from stainless steel to Zircaloy. Besides providing neutrons for diffraction experiments and radiography, an ambitious materials irradiation program STIP [2] is undertaken. Thousands of material test samples were put into special rods of the spallation target and exposed to proton and neutron irradiation at different radiation doses and temperatures, depending on their respective position in the target. Here we report a special non-destructive testing procedure used for the post-irradiation examination of the highly activated lead and STIP sample rods: the thermal neutron radiography and tomography using a remotely controlled and heavily shielded

* Corresponding author. Tel.: +41 56 310 3687; fax: +41 56 310 3131.
E-mail address: peter.vontobel@psi.ch (P. Vontobel).

0022-3115/$ - see front matter © 2006 Elsevier B.V. All rights reserved.
doi:10.1016/j.jnucmat.2006.05.033

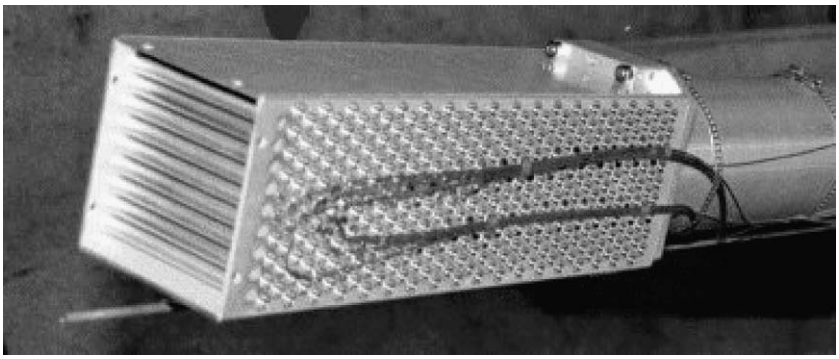

Fig. 1. SINQ Target-5, design type Mark III, array of steel cladded lead rods in aluminium cradle.

sample manipulator together with a newly developed, direct background suppressing neutron imaging plate.

2. Neutron radiography measurements

Selected lead and STIP rods from SINQ Target-5 were extracted from the target assembly five months after the end of proton irradiation. They were irradiated in the years 2002 and 2003 with an integrated proton charge of 10.85 Ah. Neutron radiography measurements were taken 11 months after the end of irradiation in mid November and beginning of December 2004. During this time the sample radioactivity was reduced by more than a factor of 10. Nevertheless, at the time of investigation, the rods were still highly radioactive (typically some 10 Sv/h in 10 cm distance) and could only be transported and manipulated in heavily shielded casks. The high remaining activity together with the material composition of the rods (lead in steel cladding) make thermal neutron radiography the preferred method for non-destructive analysis. Thermal neutrons penetrate lead quite easily because of its low linear attenuation coefficient of 0.38 cm^{-1}. The cylindrical target rods have an inner diameter of 9.8 mm, and the steel cladding has a thickness of 0.5 mm. The thermal neutron radiography facility NEUTRA at PSI has been designed for radioactive material investigations. The special shielding and manipulation setup NEURAP for radiography has been described earlier [3,4]. The high sample activity not only complicates sample manipulation but also limits the choice of a position sensitive neutron detector system for the neutron radiography investigation [4]. Here we report measurements using a specially developed dysprosium loaded imaging plate, which delivers improved neutron transmission images [5], and allows 3D tomography reconstruction of selected areas of interest. The radiography inspections were performed in two batches. In a first batch 15 rods for an overview: 3 rods side by side in a stack of 5 layers of rods separated by intermediate distance holders. Based on the radiography images from the first batch, 5 rods were selected for a detailed investigation. For that purpose at least 6 projections were taken at 30° angular increment, and one and a half rod were radiographed at 15° increments. The 12 projection images from 0° to 165° allowed 3D tomography reconstruction of selected areas of interest in a lead rod containing a thermocouple and a combined steel/Zircaloy cladding. In order to record the neutron transmission signal alone, i.e. without the contribution of the high background, dysprosium loaded imaging plates were used as a position sensitive neutron detector as described elsewhere [5]. The field of view mapped by one imaging plate was $40 \times 250\ mm^2$ ($W \times H$). The neutron beam collimation ratio L/D (D: diameter of neutron pinhole, L: distance between pinhole and imaging plane), describing the beam divergence, was 350, which led to a geometric imaging unsharpness of 0.1 mm, taking into account a sample to detector distance of 35 mm. The neutron exposure time was 25 min with a neutron flux of 6.3×10^6 $n/cm^2/s$ at the sample position. After neutron exposure the imaging plate was erased by neon light for 15 min in order to remove the induced photo-stimulated luminescence due the direct radiation from the radioactive samples. Thereafter the net neutron transmission signal was retrieved during 2 h self-exposure of the imaging plate enclosed in a light tight box by the decaying Dy-165 ($T_{1/2} = 2.33$ h) and subsequently read out in the imaging plate scanner [5].

3. Neutron radiography results

The imaging plate data sets have 16bit dynamic range and are read out by the scanner with a nominal pixel size of 50 μm. The photo-stimulated luminescence values are proportional to the neutron transmission: bright areas show the high neutron transmission regions, dark areas indicate low neutron transmission either due to increasing material penetration length and/or changing material composition (see Fig. 2). Because lead is quite transparent for thermal neutrons, the steel cladding and end caps (linear attenuation coefficient 1.1 cm^{-1}) and the thermocouple are clearly visible. The slightly higher neutron attenuation towards the center of the lead rod is due to the Gaussian like irradiation profile of the proton beam [6] inducing higher spallation product concentrations in the rod center. As described in detail in the following section a combined proton and neutron transport simulation with FLUKA [7] and/or MCNPX [8] can trace back this higher neutron attenuation mainly to an increased concentration of Hg-196 and Hg-199. These two stable mercury isotopes have rather high thermal neutron cross sections (3080 barn and 2150 barn respectively, with 1 barn = 10^{-24} cm^2), which makes small concentration differences between the center and the end visible in the thermal neutron radiography. Other effects, which are revealed by neutron radiography, are the inhomogeneous distribution of lead due to thermal expansion/shrinking or partly melting and re-solidification.

4. Comparison of radiography measurements with Monte Carlo simulations

Neutron radiography measurements were supported by Monte Carlo calculations using the FLUKA code, version 2003.1b [7]. An existing model of the SINQ facility was used. Some modifications were performed to the geometry in order to study the production of residual nuclei in a given rod, following the irradiation from the proton beam. The detailed geometry of SINQ Target-5 was considered in the model. Simulations were carried out using a measured beam profile [6]. A total history of 6×10^6 events was generated to get a good statistical accuracy. We concentrated our attention on three lead rods at different levels in the target for which neutron radiography measurements were performed. These three rods were segmented into 10 parts so that the distribution along their length could be calculated. The irradiation history of SINQ Target-5 was considered in the calculations. We assumed a continuous irradiation of 600 days with a current of 0.75 mA, followed by a radioactive decay period of 10 months. The calculation proceeded in the following way: from the FLUKA part of the calculation the residual nuclei production (in units of atoms/proton) was obtained. After that, the buildup of the isotopic inventory during the irradiation, followed by the decay was calculated using the ORIHET3 code [9]. A complete nuclide inventory was obtained for the three rods under consideration. For the interpretation of the neutron radiography results we are interested in the concentration of isotopes of high thermal neutron cross section. From the calculation results the possible isotopes with high capture cross sections are Hg-196,-199,-200,-201, Au-197, Pt-190, Os-184,-187. As an example, concentrations for the rod in the center of the target are listed in Table 1. Hg-196 and Hg-199 account for about 90% of the additional thermal neutron absorption after proton irradiation and radioactive decay. A transmission profile derived from a thermal neutron radiography along the rod axis is compared with the FLUKA simulations in Fig. 3. This was done using the Hg-196 and Hg-199 isotope concentrations calculated by FLUKA together with the nominal neutron cross section values at 0.025 eV taken from [10].

5. Neutron tomography measurements and results

Some rods of SINQ Target-5 have a mixed steel (outside)/Zircaloy (inside) cladding of 0.5 mm wall thickness for each material, which allows to investi-

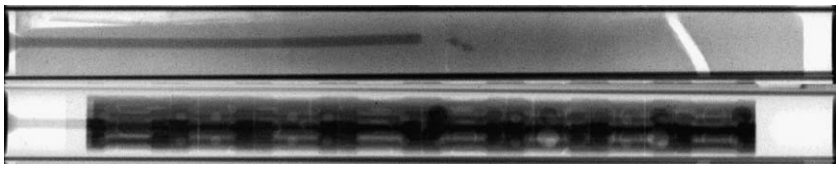

Fig. 2. Overview neutron radiographies of a lead rod (top), a STIP sample rod (bottom).

Table 1
Mass of spallation product isotopes with high thermal neutron attenuation cross section in a lead rod, calculated for a cylindrical volume of 0.9 cm^3 of lead at 90% of the nominal density

Isotope	σ [barns] 0.025 eV	Mass (grams)
^{196}Hg	3080	4E-3
^{199}Hg	2150	5E-3
^{200}Hg	<60	6E-3
^{201}Hg	<60	6E-3
^{197}Au	99	5E-3
^{190}Pt	150	2E-4
^{184}Os	3000	5E-4
^{187}Os	200	8E-4

gate lead/Zircaloy interactions under proton and neutron irradiation. Zircaloy-clad lead rods are expected to increase the neutron yield compared to steel clad rods and are tested in the actual SINQ Target-6. Strong neutron absorption spots are visible in the radiograph of this rod with mixed cladding. From a selected region of interest (Fig. 4) a 3D tomography reconstruction was performed. By this method the location, size and shape of the spots can be determined. Twelve radiography projection images were taken from this rod, rotated over 180° in angular increments of 15°. Although this was an insufficient number for angular sampling using conventional tomography reconstruction methods [11], we were able to reconstruct those regions of interest. Individual projections had first to be aligned along the rotation axis, the tilt of the rotation axis had to be corrected and the images had to be centered. These are necessary conditions for reconstruction, which are usually satisfied when using a stationary CCD camera setup for tomography. The here applied imaging plate detector setup was not a stationary device. The changing location and tilt of the rod projections on the image matrix were therefore corrected using one-dimensional and two-dimensional image correlation methods. Inhomogeneities in the dysprosium loaded imaging plates like small scratches or less neutron sensitive spots had to be corrected manually. Neutron exposure normalization of radiographs was required due to the unsteady proton current. This was performed averaging a rectangular area of interest at the left and right border of the projection image. The corrected images were stored in a volume data set, from which slices perpendicular to the rod rotation axis were reconstructed using a special Fourier transform based inversion scheme called 'GridRec'. This algorithm was implemented by G.H. Campbell and R.B. Marr [12] and made available in an IDL (http://www.rsinc.com) based reconstruction package by M. Rivers [13]. The reconstructed central area of interest is shown in the upper part of Fig. 4. On the flat side the spot diameter is about 1 mm. We assume that these image spots originate from strongly neutron scattering ZrH_2 in the Zircaloy. These Zr hydrides are brittle enclosures in the Zircaloy and could cause cladding failure. This type of cladding degradation has been studied for many decades in the nuclear industry, see e.g. [14] for a recent investigation. Fig. 5 shows a cross section through the lead rod with zirconium hydride lenses.

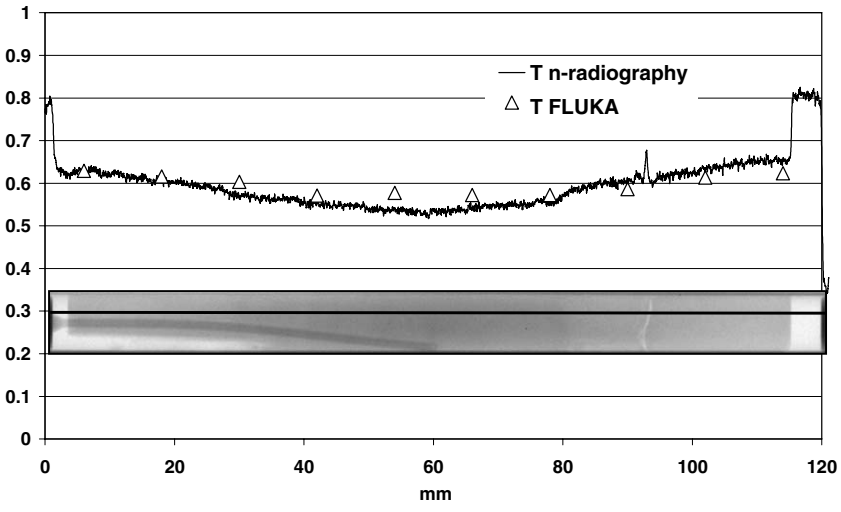

Fig. 3. Comparison of measured neutron transmission with simulated data from FLUKA for a lead rod.

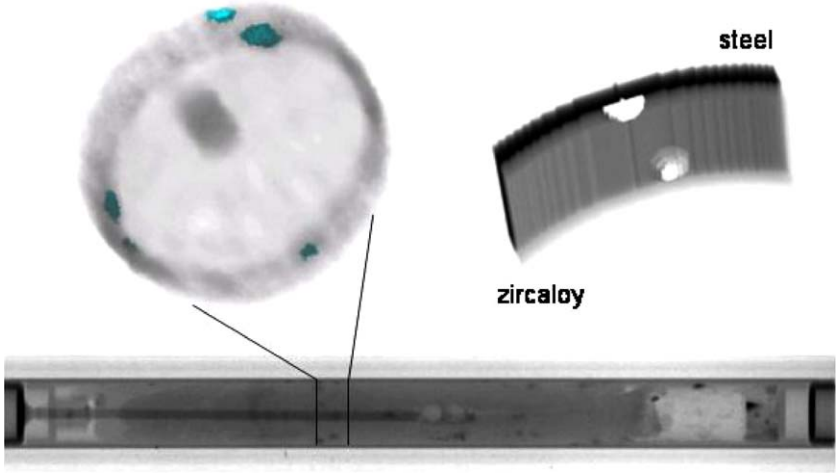

Fig. 4. Strongly neutron attenuating ZrH_2 lenses in a lead rod with combined steel/Zircaloy cladding. N-radiography (bottom), selected region of interest in 3D view and schematic representation of the steel/Zircaloy interface (top).

The shape of the spots is flat towards the steel/Zircaloy contact surface and has a convex shape inside the Zircaloy cladding. Although there is quite a lot of noise and image blurring in this single reconstructed slice, it shows that the flat base of the lens is sitting at the steel/Zircaloy interface and the concavity points towards the rod center. The question from which side, i.e. either from the outer steel cladding or from the lead in the rod, the hydride lenses are growing cannot be answered from the neutron tomography alone. The small number of angular projections used for the reconstruction together with the high noise level make a precise determination of the location of the spot within the Zircaloy wall impossible. From the radiography data however the exact position within the rod for a destructive analysis can be determined. This is a big advantage for analyzing radioactive samples.

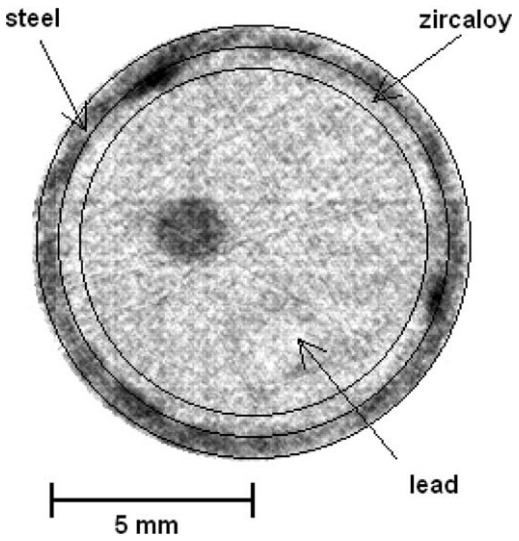

Fig. 5. Neutron tomography slice of lead rod through ZrH_2 spots: thermocouple inside rod, ZrH_2 lenses in Zircaloy at steel/Zircaloy interface.

6. Summary and conclusion

Thermal neutron radiography and tomography have been applied for non-destructive investigation of highly radioactive lead spallation target rods. The heat load applied during proton irradiation has an impact on the spatial distribution of lead filled into the steel tubes. The weakly decreasing thermal neutron transmission along the rod axis can be attributed to the varying Hg-196 and Hg-199 spallation product concentrations caused by the shape of the proton beam. This has been verified by a Monte Carlo simulation of the proton and neutron transport in SINQ Target-5 and a subsequent activation calculation considering the integrated proton current over two years irradiation and a 10 months radioactive decay time. Metal hydride formation could only be detected in a mixed steel/Zircaloy clad lead rod, where ZrH_2 lenses cause strong thermal neutron attenuation in the Zircaloy tube wall. The size and location of the Zircaloy hydride spots can be identified by neutron radiography/-tomography, which indicate the places for further destructive testing. In rods clad by steel only, no spatially varying hydrogen concentration could be detected by thermal neutron radiography/tomog-

raphy. Although the hydrogen production in the steel and lead is about 3–5 times higher than the mercury production (according to Monte Carlo simulations using the MCNPX code), the much lower thermal neutron cross section of hydrogen (82 barn) does not provide enough contrast in the radiography when hydrogen is evenly distributed and not concentrated in localized spots.

Acknowledgements

We thank Gabriel Frei and George Necola for support during the radiography measurements and radiography image processing. Michael Wohlmuther provided hydrogen concentrations calculated by MCNPX.

References

[1] G.S. Bauer, Nucl. Instrum. and Meth. B 139 (1–4) (1998) 65.
[2] Y. Dai, G.S. Bauer, J. Nucl. Mater. 296 (1–3) (2001) 43.
[3] F. Gröschel, P. Schleuniger, A. Hermann, E. Lehmann, L. Wiezel, Nucl. Instrum. and Meth. A 424 (1999) 215.
[4] E. Lehmann, P. Vontobel, M. Estermann, Appl. Radiat. Isot. 61 (2004) 603.
[5] M. Tamaki, K. Iida, N. Mori, E.H. Lehmann, P. Vontobel, M. Estermann, Nucl. Instrum. and Meth. A 542 (1–3) (2005) 320.
[6] U. Rohrer, p-Strahlbreiten und Profil-Formen beim SINQ-Target mit und ohne Target E (4 cm Graphit), PSI internal report, 2001.
[7] A. Fasso, A. Ferrari, J. Ranft, P.R. Sala, FLUKA, in: Proceedings of Monte Carlo 2000, Lisbon, 23–26 October 2000, Springer, Berlin, 2001, p. 159, 955.
[8] L.S. Waters (Ed.), MCNPX User's Manual Version 2.4.0, Los Alamos National Laboratory report LA-CP-02-408, September 2002.
[9] F. Atchison and H. Schaal, ORIHET 3 - Version 1.12, A guide for users, PSI internal report, March 2001.
[10] V.F. Sears, Neutron News 3 (1992) 26. Available from: <http://www.ncnr.nist.gov/resources/n-lengths/>.
[11] A.C. Kak, M. Slaney, Principles of Computerized Tomographic Imaging, SIAM, 2001, ISBN 0-89871-494-X. Available from: <www.slaney.org/pct>.
[12] B.A. Dowd, G.H. Campbell, R.B. Marr, et al., Developments in synchrotron X-ray computed microtomography at the national synchrotron light source, in: SPIE Conf. on Developments in X-Ray Tomography II, Denver, Colorado, 1999.
[13] M. Rivers, IDL Software for tomography: http://cars9.uchicago.edu/software/idl/tomography.html.
[14] S.I. Hong, K.W. Lee, J. Nucl. Mater. 340 (2005) 203.